Greater variability in local vegetation structure increases forest resistance to wildfire

Michael J Koontz[1], Malcolm P North[1, 2], Stephen E Fick[3], Chhaya M Werner[4], and Andrew M Latimer[1]

[1]*Graduate Group in Ecology, University of California, Davis, CA 95616 USA*
[2]*USDA Forest Service, Pacific Southwest Research Station, Davis, CA 95618 USA*
[4]*Stockholm Environment Institute, Stockholm 115 23, Sweden*
[5]*Center for Population Biology, University of California, Davis, CA 95616 USA*

Abstract. Variation in the size and distribution of trees can enable a forest to withstand ongoing disturbances and retain its essential identity and function. We test this phenomenon at a broad spatial extent in California's Sierra Nevada region using remotely-sensed data corroborated with on the ground measurements. We find that greater heterogeneity in local forest structure reduces the severity of wildfires. Heterogeneous forest structure thus makes mixed conifer forest in the Sierra Nevada more resistant to this inevitable disturbance, and may increase the probability of its long-term persistance. Management activities that seek to increase forest heterogeneity, such as prescribed fire, should be continued.

Key words: resilience; *wildfire severity*; *RdNBR*; *remote sensing*

Introduction

Three intertwining themes:

1. Resilience of disturbance-prone (e.g., wildfire) systems is important basic ecological question with dramatic socio-ecological consequences. We can measure part of resilience by recognizing panarchy and measuring how heterogeneous vegetation promotes forest resistance at very broad scales.
2. We can measure severity in a programmatic way to get comparable data across broader spatial and deeper temporal extents.
3. We can apply texture analysis to vegetation to quantify heterogeneity.

Biological systems comprising heterogeneous elements can retain their fundamental properties in the face of regular disturbance. This ability of a heterogeneous system to absorb disturbances, reorganize, and to persist within a domain of stability with respect to its identity, structure, function, and feedbacks is termed resilience (Holling 1973; Gunderson 2000; Folke *et al.* 2004; Walker *et al.* 2004). Resilience (*sensu* Walker *et al.* (2004)) is characterized by four critical features: 1) latitude, which describes the degree to which a system can deviate from an attracting state and still recover to that state, 2) resistance, which describes the intensity or duration of a disturbance required to change the system state, 3) precariousness, which describes the proximity of a system to a threshold of a different domain of stability, and 4) panarchy, which describes how resilience features interact across multiple scales of organization. Resilience has been demonstrated in complex biological systems characterized by a variety of different types of "heterogeneity" including genetic diversity (Reusch *et al.* 2005; Agashe 2009; Baskett *et al.* 2009), species diversity (Tilman 1994; Chesson 2000;

Cadotte *et al.* 2013), functional diversity (Gazol & Camarero 2016), topoclimatic complexity (Ackerly *et al.* 2010, @Lenoir2013), and temporal environmental variation (Questad & Foster 2008). An emerging paradigm in forest ecology is that spatial heterogeneity in the structure of vegetation on the landscape can confer resilience to disturbances such as wildfire, drought, and insect outbreaks (Stephens *et al.* 2008; North *et al.* 2009; Virah-Sawmy *et al.* 2009). Forests are globally important ecosystems threatened in a number of ways, and protection of forests is of high management priority (Hansen *et al.* 2013; Crowther *et al.* 2015; Millar & Stephenson 2015; Trumbore *et al.* 2015). Thus, it is critical to understand the mechanisms underlying the effect of spatial heterogeneity in forest structure on forest resilience.

Forest structure is defined by the size and distribution of trees on the landscape. Differences in tree crown heights characterize vertical structure, while differences in the rooting locations of trees characterizes horizontal structure (North *et al.* 2009). Structural patterns can be further parsed by the constituent species present. In the Sierra Nevada range of California, forests are dominated by a mixture of conifer species including ponderosa pine (*Pinus ponderosa*), sugar pine (*Pinus lambertiana*), incense-cedar (*Calocedrus decurrens*), Douglas-fir (*Pseudotsuga menziesii*), white fir (*Abies concolor*), and red fir (*Abies magnifica*) (Stephens & Collins 2004; Collins *et al.* 2015). Tree density in the early 20th century was relatively low, with about 25-79 trees/ha and about 8-30 m2/ha of live basal area (Collins *et al.* 2015). Previous work described the historical distribution of trees in the Sierra Nevada as an "ICO pattern," which refers to its three distinct features: individual trees (I), clumps of trees with interlocking crowns (C), and openings with no tree cover at all (O) (Larson & Churchill 2012). The ICO pattern manifests at small spatial extents between 0.2 and 1.2 ha and is maintained by feedbacks with spatially explicit ecological processes (Larson & Churchill 2012; Lydersen *et al.* 2013; Fry *et al.* 2014). Competition for light, water, and other resources can yield aggregations of trees within favorable microsites or more widely spaced trees to ameliorate detrimental interactions (Clyatt *et al.* 2016). Demographic processes of dispersal, recruitment, and mortality affect forest structure by adding or subtracting whole trees. Reciprocally, the forest structure can also influence these pattern-forming processes such as when vegetation overstory alters microclimate or changes tree demographic rates (Larson & Churchill 2012; De Frenne *et al.* 2013; Ford *et al.* 2013). The stabilizing effects of these reciprocal processes in forests are hallmarks of a resilient system (Folke *et al.* 2004). In the Sierra Nevada range of California, the strongest feedbacks between forest structure and pattern-generating ecological process relate to the widespread disturbances caused by wildfire and bark beetle outbreaks (Raffa *et al.* 2008; Larson & Churchill 2012; Millar & Stephenson 2015). Wildfire and bark beetle outbreaks both kill live trees, affect hundreds of thousands to millions of hectares of forested area per year, and interact dynamically with the forest structures they encounter (Westerling *et al.* 2006; Raffa *et al.* 2008; Larson & Churchill 2012; Park Williams *et al.*

2012).

In an ecological framework, wildfire is typically classified into different fire regimes that describe how frequently and how intensely they burn (Keeley *et al.* 2011; Mandle *et al.* 2011; Steel *et al.* 2015). For instance, mixed conifer forests in the Sierra Nevada burned every 11 years on average for several centuries prior to Euro-American settlement (Steel *et al.* 2015). These relatively frequent burns prevented the accumulation of fuel on the ground, and limited the intensity of the next fire. This average fire return interval is short compared to the regeneration time of the dominant species, so the fire regime of Sierra Nevada mixed conifer forests in this period is usually classified as a "high frequency/low-mid severity" (Steel *et al.* 2015). However, wildfire behavior is inherently complex and is influenced by local weather, topography, and heterogeneous fuel conditions created by departures from the average fire return interval at any particular place (Sugihara & Barbour 2006; Collins & Stephens 2010). Wildfire can affect the future forest structure by changing demographic rates of individual trees (e.g. increasing growth or germination via increasing light or nitrogen availability), but it's most lasting impact to forest structure is in the pattern of killed trees left in its wake (Larson & Churchill 2012). Reciprocally, forest structure can influence fire behavior: for instance, high tree density and presence of "ladder fuels" in the understory increase the probability of crown fire that kills a high proportion of trees (Stephens *et al.* 2008; North *et al.* 2009).

Severity describes the effect of a wildfire on an ecosystem– often the amount of vegetation mortality (Sugihara & Barbour 2006). Wildfire severity can be measured by comparing pre- and post-fire satellite imagery for a specific area, but this usually requires considerable manual effort for image collation and processing, followed by calibration with field data (Miller & Thode 2007; Miller *et al.* 2009; De Santis *et al.* 2010; Cansler & McKenzie 2012; Veraverbeke & Hook 2013; Parks *et al.* 2014; Prichard & Kennedy 2014; Edwards *et al.* 2018; Fernández-García *et al.* 2018). Efforts to measure severity across broad spatial extents, such as the Monitoring Trends in Burn Severity project (Eidenshink *et al.* 2007), are unsuitably subjective for rigourous scientific analysis though they serve their intended management purpose admirably (Kolden *et al.* 2015). Automated efforts to remotely assess wildfire have arisen, but they tend to focus on more aggregate measures of wildfire such as whether an area burned or the probability that it burned rather than the severity of the burn (Bastarrika *et al.* (2011); Goodwin & Collett (2014); Boschetti *et al.* (2015); Hawbaker *et al.* (2017) but see Reilly *et al.* (2017)). Here, we present a method to automate the measurement of wildfire severity using minimal user inputs: a geometry of interest (a wildfire perimeter or a field plot location) and an alarm date (the date the fire began). This information is readily available in many fire-prone areas (such as California, via the Fire and Resource Assessment Program; http://frap.fire.ca.gov/projects/fire_data/fire_perimeters_index) or could potentially be derived using existing products (such as the Landsat Burned Area Essential Climate

Variable product described in Hawbaker *et al.* (2017)). Further, the flexibility of this approach faciliates collaborative calibration with field-collected wildfire severity data.

Vegetation characteristics such as canopy density (Rouse *et al.* 1973; Young *et al.* 2017), moisture content (Asner *et al.* 2015), insect attack (Näsi *et al.* 2015), and even functional diversity (Asner *et al.* 2017) can be measured using remotely-sensed imagery. Texture analysis of imagery can quantify ecologically relevant environmental heterogeneity across broad spatial scales (Wood *et al.* 2012). Texture analysis was originally developed for image classification and computer vision, and it characterizes each pixel in an image by a summary of its neighboring pixels (Haralick *et al.* 1973; Conners *et al.* 1984). Ecologists have successfully used texture measurements to augment predictions of species richness (Huang *et al.* (2014); Stein *et al.* (2014); Tuanmu & Jetz (2015) but see Culbert *et al.* (2012)).

Resilience has gained new attention in light of anthropogenic global change because of the potential for novel disturbance regimes to exceed a system's capacity to recover (Millar *et al.* 2007; Turner *et al.* 2013). Beyond these thresholds, catastrophic shifts in ecosystems are likely, with myriad consequences for ecosystems and the services they provide (Scheffer *et al.* 2001; Turner *et al.* 2013). Changes in wildfire disturbance regimes are particularly suited to catalyze catastrophic shifts in ecosystems because of their feedback with spatial forest heterogeneity at multiple scales. Anthropogenic global change and a century of fire suppression policy in the United States have resulted in forest conditions far outside their range of historic variability, with potentially dire consequences for society (North *et al.* 2015). In California, increasing temperature couples with increasing drought frequency to exacerbate water stress and drive tree mortality during "hotter droughts" (Park Williams *et al.* 2012; Millar & Stephenson 2015). Further, a century of fire suppression policy has led to drastic changes in forest structure (North *et al.* 2015). Canopy cover has increased by 25-49%, overall tree density has increased by >75%, and white fir (*Abies concolor*) makes up a greater percentage of basal area compared to forests in the early 20th century (Stephens *et al.* 2015). The change in tree density is underlaid by a shift in size distribution: modern mixed conifer forests have 2.5 times as many trees between 30.4 and 61.0cm diameter at breast height (dbh) per hectare (103.9 versus 41.0 trees/ha) and half as many trees greater than 91.4cm dbh per hectare (8.7 versus 16.7 trees/ha) compared to forests in 1911 (Stephens *et al.* 2015). Thus, western North American forests are experiencing novel, "unhealthy" conditions (*sensu* Raffa *et al.* (2009)) that are liable to upset the feedbacks between forest structure and pattern-forming ecological disturbances that historically stabilized the system and made it resilient (Raffa *et al.* 2008; Millar & Stephenson 2015).

A forest that is resistant to wildfire will be less impacted following a disturbance of that type. In forests with relatively intact fire regimes and heterogeneous stand conditions such as in the Jeffrey pine forests of the

Sierra San Pedro Martir in Baja, California, there tends to be reduced vegetation mortality after wildfires compared to fire-suppressed forests (Stephens *et al.* 2008). A heterogeneous forest can largely avoid overstory tree mortality because a reduced amount of accumulated ladder fuel decreases its ability to get into the crown (where mortality is more likely to result), because widely-spaced tree clumps interrupt fire spread across the landscape, and because tree clumps with fewer trees don't facilitate self-propagating fire behavior (Graham *et al.* 2004; Scholl & Taylor 2010). Thus, forests with heterogeneous structure are predicted to persist in that state due to resistance to inevitable wildfire disturbance (Graham *et al.* 2004; Moritz *et al.* 2005; Stephens *et al.* 2008). However, it is unclear whether this is true at broad spatial extents, nor is it resolved at what scale heterogeneity in forest structure is meaningful for resilience (Kotliar & Wiens 1990).

Does spatial variability in forest structure confer resilience to California mixed conifer forests by reducing the severity of wildfires when they occur?

Methods

This work occurred in two phases. First, we developed a new approach to calculating wildfire severity across broad spatial and temporal scales and calibrated our measurements to those frome the field. We applied this approach to all known fire perimeters in the Sierra Nevada region between 1984 and 2016 as defined by the Fire and Resource Assessment Program (FRAP, http://frap.fire.ca.gov/projects/fire_data/fire_perimeters_index), which is the most comprehensive digital record of fire occurrence in California. Second, we used texture analysis of remotely-sensed imagery bounded by the perimeters in the FRAP database to develop a measure of vegetation heterogeneity and modeled how that heterogeneity affected wildfire severity, accounting for other key drivers of wildfire behavior.

Study area

Yellow pine and mixed conifer forests of Sierra Nevada, California between 1984 and 2016.

A new approach to remotely sensing wildfire severity

Wildfire severity can be reliably detected remotely by comparing pre- and postfire imagery from sensors aboard the Landsat series of satellites (Eidenshink *et al.* 2007; Miller & Thode 2007). The Thematic Mapper (TM; Landsat 4 and 5), Enhanced Thematic Mapper Plus (ETM+; Landsat 7), and Operational Land Imager

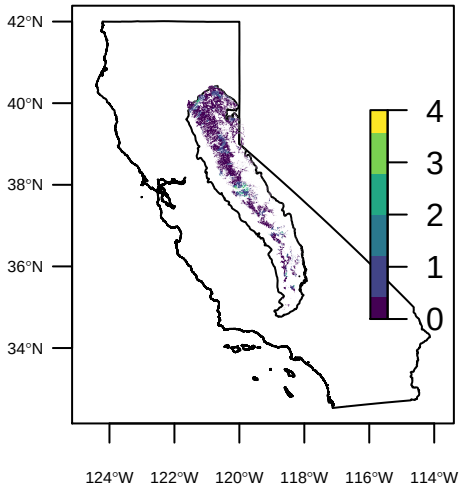

Figure 1: Locations of fires in yellow pine/mixed conifer forests in the Sierra Nevada mountain range of California. Colored pixels are designated yellow pine/mixed conifer according to the presettlement fire regime from the FRID database. Colors represent the number of fires that burned in that area during the satellite era.

(OLI; Landsat 8) sensors generate compatible top-of-atmosphere (TOA) spectral reflectance data suitable for scientific analysis. Recent advances in radiometric correction post-processing can compensate for various atmospheric distortions and generate more accurate measurements of surface reflectance in narrow wavelength bands spanning the electromagnetic spectrum (Masek *et al.* 2006; Vermote *et al.* 2016; USGS 2017b, a). Landsat satellites image the entire Earth approximately every 16-days and repeat images of the same area are geometrically coregistered such that overlapping pixels correspond to the same area on the ground. We used Google Earth Engine, a cloud-based geographic information system and image hosting platform, for all image collation and processing in order to leverage the centralized availability of the latest processed satellite images and integrated image processing tools for broad-scale analyses (Gorelick *et al.* 2017).

The base assumption of our new approach to calculating wildfire severity is that each fire's geographic data and associated attributes are represented by a self-contained "feature". Many fire datasets (e.g., FRAP, USFS Region 5 Fire Perimeter Data, CBI field plot locations from Zhu *et al.* (2006) and Sikkink *et al.* (2013)) already meet this criteria. In order to achieve a programmatic, automatic assessment of wildfire severity, severity-calculating algorithms must be able to use only the information within each feature. Time efficiencies and data compatibility benefits are attained when those algorithms are applied across an entire feature collection, performing their operation on each feature in turn. At a minimum, our algorithm requires that each feature contain some geographic information (e.g., a fire perimeter or a cbi plot location) and a fire start date (i.e., an "alarm date").

Fetching and processing pre- and postfire imagery

All Landsat imagery was fetched by "scene"– the atomic unit of image data in the Landsat collection representing an area on the Earth's surface approximately 170 km long by 183 km wide. For each feature, a collection of Landsat scenes was fetched both before and after the fire by defining a date range to search for imagery. The date range for prefire imagery started one day before each feature's alarm date and extended backward in time by a user-defined time window. The date range for postfire imagery was exactly one year after the date range for the prefire search (i.e., one year after the day before the fire, extending backward in time by the same time window). We tested 4 time windows: 16, 32, 48, or 64 days which were chosen to ensure that at least 1, 2, 3, or 4 Landsat images, taken on a 16-day interval, were captured by the date ranges (Fig. 2).

The Landsat archive was filtered to generate a prefire image collection comprising only the Landsat scenes depicting some part of the feature geometry and within the prefire date range. A postfire image collection

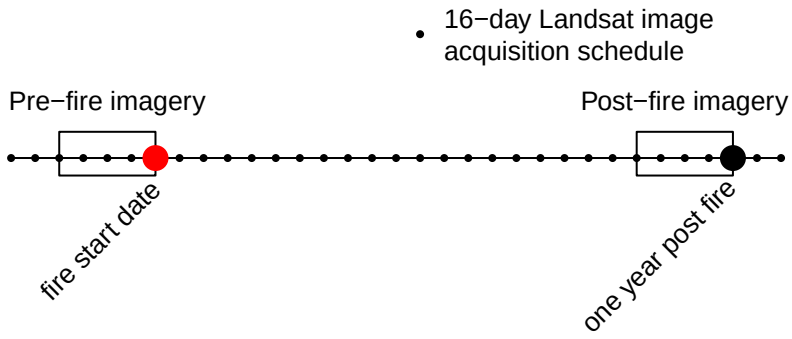

Figure 2: Schematic for how Landsat imagery was assembled in order to make comparisons between pre- and post-fire conditions. This schematic depicts a 64-day window of image collation prior to the fire which comprise the pre-fire image collection. A similar, 2-month window collection of imagery is assembled one year after the pre-fire image collection.

was similarly generated by filtering the Landsat archive by the postfire date range and the feature geometry. The Landsat archive we filtered included imagery from Landsat 4, 5, 7, and 8, so each pre- and postfire image collection may contain a mix of scenes from different satellite sources to enhance coverage.

For each image in the pre- and postfire image collections, we masked pixels that were not clear (i.e., clouds, cloud shadows, snow, and water) and calculated standard indices that capture vegetation cover and fire effects such as charring: normalized difference vegetation index (NDVI; Rouse *et al.* (1973)), normalized difference moisture index (NDMI; Gao (1996)), normalized burn ratio (NBR; Key & Benson (2006); USGS (2017a); USGS (2017b)), and normalized burn ratio version 2 (NBR2; USGS (2017a); USGS (2017b); Hawbaker *et al.* (2017)) following Eq. 1:

$$\begin{aligned} NDVI &= (NIR - RED)/(NIR + RED) \\ NDMI &= (NIR - SWIR1)/(NIR + SWIR1) \\ NBR &= (NIR - SWIR2)/(NIR + SWIR2) \\ NBR2 &= (SWIR1 - SWIR2)/(SWIR1 + SWIR2) \end{aligned} \tag{1}$$

Where NIR is the near infrared band (band 4 on Landsat 4, 5, and 7; band 5 on Landsat 8) and RED is the red band (band 3 on Landsat 4, 5, and 7; band 4 on Landsat 8), SWIR1 is the first short wave infrared band (band 5 on Landsat 4, 5, and 7; band 4 on Landsat 8), SWIR2 is the second short wave infrared band (band 7 on Landsat 4, 5, 7, and 8)

We summarized each prefire image collection into a single prefire image using a median reducer, which calculated the median of the unmasked values on a per-pixel basis across the stack of images in the prefire

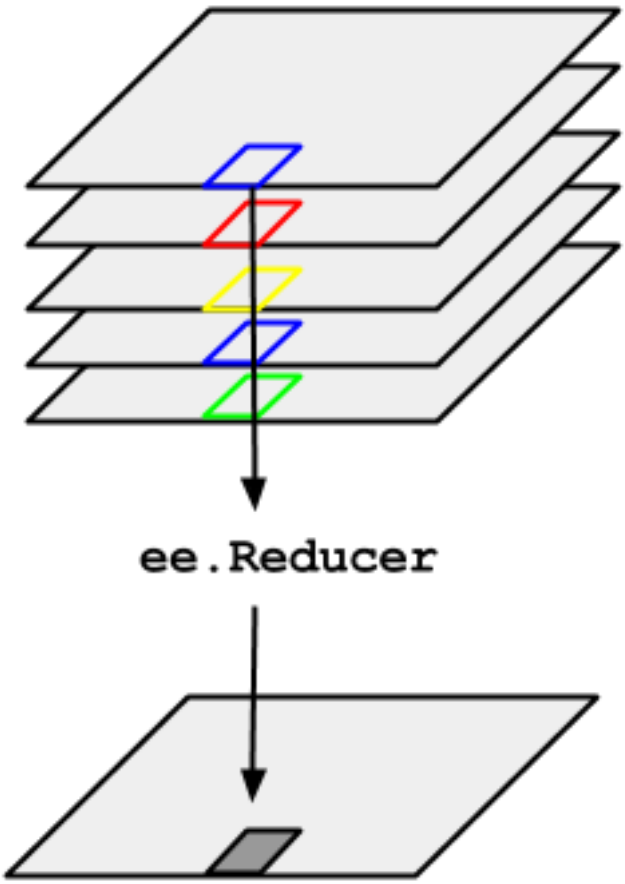

Figure 3: Reductions of an image collection that characterize each pixel as a summary statistic of a stack of corresponding pixels at different points in time. In our case we summarize a time series of each pixel into the median value across that series. Image courtesy of Google and can be found at https://developers.google.com/earth-engine/reducers_image_collection

collection. We similarly summarized the postfire image collection into a single postfire image (Fig. 3).

Calculating wildfire severity

We calculated remotely-sensed wildfire severity using the relative burn ratio (RBR) (Parks *et al.* 2014), the delta normalized burn ratio (dNBR) (Eidenshink *et al.* 2007; Miller & Thode 2007), the relative delta normalized burn ratio (RdNBR) (Miller & Thode 2007), the delta normalized burn ratio 2 (dNBR2) (Hawbaker *et al.* 2017), the relative delta normalized burn ratio 2 (RdNBR2), and the delta normalized difference vegetation index (dNDVI) (Eidenshink *et al.* 2007). Following the success of the RdNBR metric in other studies, we also calculate an analogous metric using NDVI– the relative delta normalized difference vegetation index (RdNDVI).

We calculated the delta severity indices by subracting the postfire index from the prefire index without multiplying by a rescaling constant (e.g., we did not multiply the result by 1000 as in Miller & Thode (2007)):

$$dINDEX = INDEX_{\text{prefire}} - INDEX_{\text{postfire}} \tag{2}$$

Following Reilly *et al.* (2017), we chose not to correct the delta indices using a phenological offset value (typically calculated as the delta index in homogenous forest patch outside of the fire perimeter), as our approach implicitly accounts for phenology by incorporating multiple cloud-free images across the same time window both before the fire and one year later.

We calculated the relative delta severity indices by scaling the delta index from Eq. 2 by a square root transformation of the absolute value of the prefire index:

$$RdINDEX = \frac{dINDEX}{\sqrt{|INDEX_{\text{prefire}}|}} \tag{3}$$

We calculated the relative burn ratio (RBR) following Parks *et al.* (2014):

$$RBR = \frac{dNBR}{NBR_{\text{prefire}} + 1.001} \tag{4}$$

Calibrating remotely-sensed wildfire severity with field-measured wildfire severity

We calibrated our remotely-sensed measure of wildfire severity with 208 field measures of overstory tree mortality from two previously published studies (Zhu *et al.* 2006; Sikkink *et al.* 2013) (Fig. 4). The Composite Burn Index (CBI) is a metric of change in vegetation across several vertical strata (Key & Benson 2006) and has a long history of use in calibrating remotely-sensed severity data (Miller & Thode 2007; Miller *et al.* 2009; Cansler & McKenzie 2012; Parks *et al.* 2014; Prichard & Kennedy 2014). Following Miller & Thode (2007), Miller *et al.* (2009), and Parks *et al.* (2014), we fit a non-linear model to each remotely-sensed severity metric of the following form:

$$\text{remote\_severity} = \beta_0 + \beta_1 e^{\beta_2 \text{cbi\_overstory}} \tag{5}$$

We fit the model in Eq. 5 for all 7 of our remotely-sensed severity metrics (RBR, dNBR, RdNBR, dNBR2, RdNBR2, dNDVI, RdNDVI) using 4 different time windows from which to collate satellite imagery (16, 32, 48,

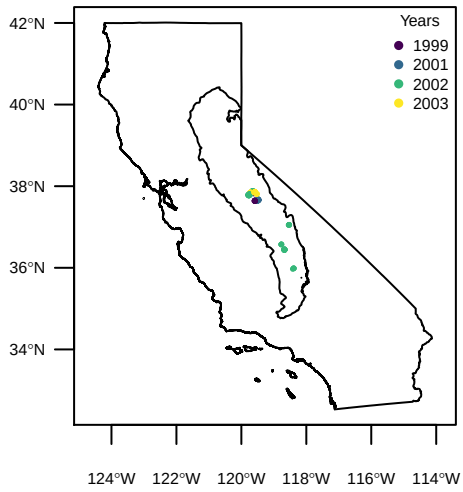

Figure 4: Location of CBI plots in the Sierra Nevada mountain range of California

and 64 days). Following Cansler & McKenzie (2012) and Parks *et al.* (2014), we used interpolation to extract remotely-sensed severity at the locations of the CBI field plots to better align remote and field measures of severity. We extracted remotely-sensed severity values using both bilinear interpolation, which returns a severity value weighted by the 9 pixel values nearest to the CBI plot location, and bicubic interpolation, which returns a severity value weighted by the 16 pixel values nearest to the CBI plot location. In total, we fit 56 models (7 severity measures, 4 time windows, 2 interpolation methods) and performed five-fold cross validation using the `modelr` and `purrr` packages. To compare goodness of model fits with Miller & Thode (2007), Miller *et al.* (2009), and Parks *et al.* (2014), we report the average R^2 value from the five folds for each of the 56 models but note that R^2 for non-linear regressions do not have the same interpretation that they do for linear regression (i.e., R^2 can be greater than 1 for non-linear regression, so it can't be interpreted as the proportion of variation explained by the model). We used the Relative Burn Ratio (RBR) calculated using bicubic interpolation within a 48-day window as our response variable for analyses of vegetation heterogeneity, as it showed the best correspondence to field severity data measured as average R^2 across the five folds.

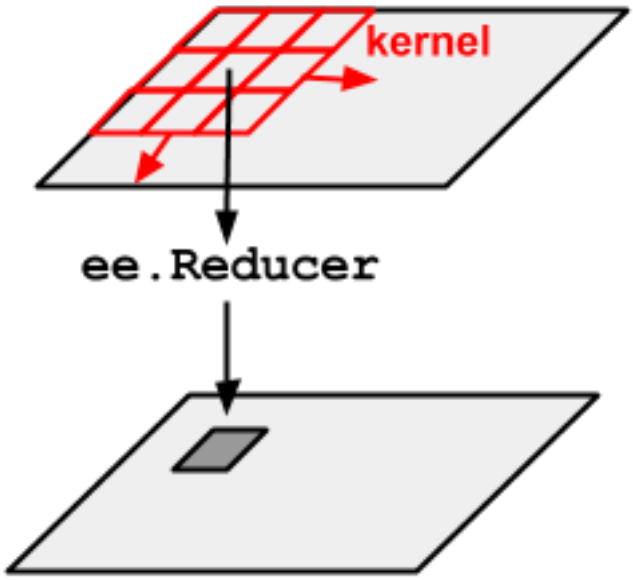

Figure 5: Neighborhood reducer that characterize each pixel as a summary of the neighboring pixels within a specified kernel. Image courtesy of Google and can be found at https://developers.google.com/earth-engine/reducers_reduce_neighborhood

Remote sensing other conditions

Heterogeneity of vegetation

We used texture analysis to calculate a remotely-sensed measure of forest heterogeneity (Haralick *et al.* 1973; Tuanmu & Jetz 2015). Within a moving square neighborhood window with sides of 90m, 150m, 210m, and 270m (corresponding to a moving neighborhood window of 0.81 ha, 2.25 ha, 4.41 ha, and 7.29 ha), we calculated heterogeneity for each focal pixel as the standard deviation of the NDVI values of its neighbors (not including itself).

Other vegetation conditions

We calculated pre-fire NDVI for each pixel.

We calculated the pre-fire mean NDVI in the same moving windows as the standard deviation of NDVI.

Topographic conditions

Elevation data were sourced from the Shuttle Radar Topography Mission (Farr *et al.* 2007), a 1-arc second digital elevation model. Slope and aspect were extracted from the digital elevation model. Per-pixel topographic roughness was calculated as the standard deviation of elevation values within a the same kernel sizes as those used for vegetation heterogeneity (approximately 90m, 150m, 210m, and 270m on a side and not including the central pixel). Some work has shown that terrain ruggedness (Holden *et al.* 2009), and particularly coarser-scale terrain ruggedness (Dillon *et al.* 2011), is an important predictor of wildfire severity.

We used the digital elevation model to calculate the potential annual heat load at each pixel, which is an integrated measure of latitude, slope, and aspect (McCune & Keon (2002) with correction in McCune (2007)).

Folding the aspect about the northeast-southwest line, such that northeast becomes 0 radians and southwest becomes π radians.

$$aspect_{folded} = |\pi - |aspect - \frac{5\pi}{4}|| \tag{6}$$

$$\begin{aligned} log(PAHL) = -1.467+ \\ 1.582 * cos(latitude) * cos(slope)- \\ 1.5 * cos(aspect_{folded}) * sin(slope) * sin(latitude)- \\ 0.262 * sin(lat) * sin(slope)+ \\ 0.607 * sin(aspect_{folded}) * sin(slope) \end{aligned} \tag{7}$$

Where PAHL is the potential annual heat load, folded_aspect is determined by Eq. 6 and is in units of radians, and both latitude and slope are extracted from a digital elevation model with units of radians.

Fire weather conditions

The 100-hour fuel moisture data were sourced from the Gridmet product (Abatzoglou 2013) and were calculated as the median 100-hour fuel moisture for the 3 days prior to the fire. We included a boolean variable for extreme values of 100-hour fuel moisture if they were lower than 7.7%, since these values fall below the 20^{th} percentile of 100-hour fuel moisture for the Sierra Nevada region (Stephens *et al.* 2013).

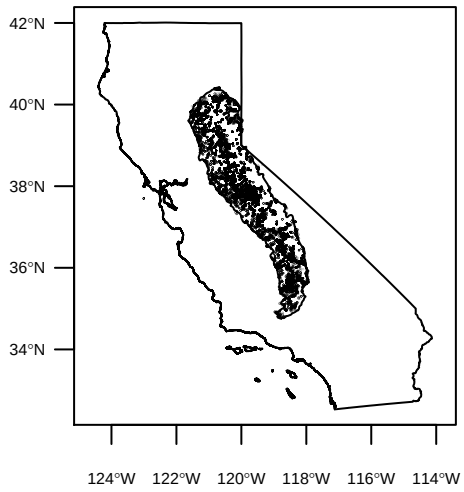

Figure 6: Locations of samples from fires in yellow pine/mixed conifer forests in the Sierra Nevada mountain range of California.

Modeling the effect of heterogeneity on severity

We scaled all predictor variables, and treated each individual fire as having a random intercept effect using the following mixed effects model:

$$\begin{aligned} severity_{i,j} &\sim \mathcal{N}(\mu_{i,j}, \sigma_{\text{error}}) \\ \mu_{i,j} &= \beta_0 + \gamma_j + \beta_{\text{heterogeneity}} * \text{heterogeneity\_i} \end{aligned} \tag{8}$$

Each neighborhood size was substituted in turn for the heterogeneity of NDVI covariate, to generate a candidate set of 4 models which were compared using AIC. The model with the best out-of-sample prediction was further analyzed by comparing the B coefficients to assess the relative effect of each predictor on wildfire severity.

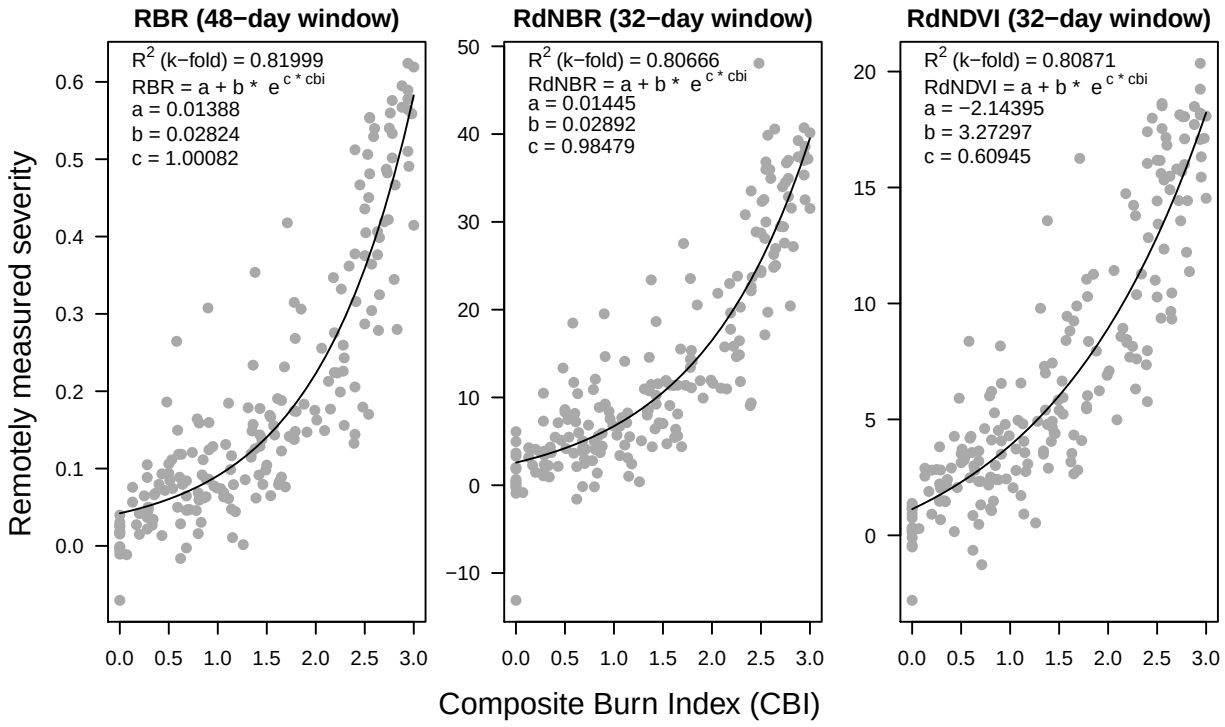

Figure 7: Calibration of three remotely-sensed severity metrics using new automated image collation algorithm to 208 field measures of severity.

Statistical software and data availability

We used `R` for all statistical analyses (R Core Team 2017). We used the `lme4` package to fit mixed effects models (Bates *et al.* 2015).

Data are available via the Open Science Framework.

Results

1. On-the-ground CBI measurements correlate well with our derived severity measurements. Our algorithm with its R^2 puts it among the best (Edwards *et al.* 2018).
2. Heterogeneity of local NDVI is a meaningful measure of heterogeneity
3. The best model used heterogeneity at the smallest spatial scale.
4. Greater heterogeneity reduces wildfire severity.
5. The relative importance of heterogeneity depends on fire weather conditions (fuel moisture).

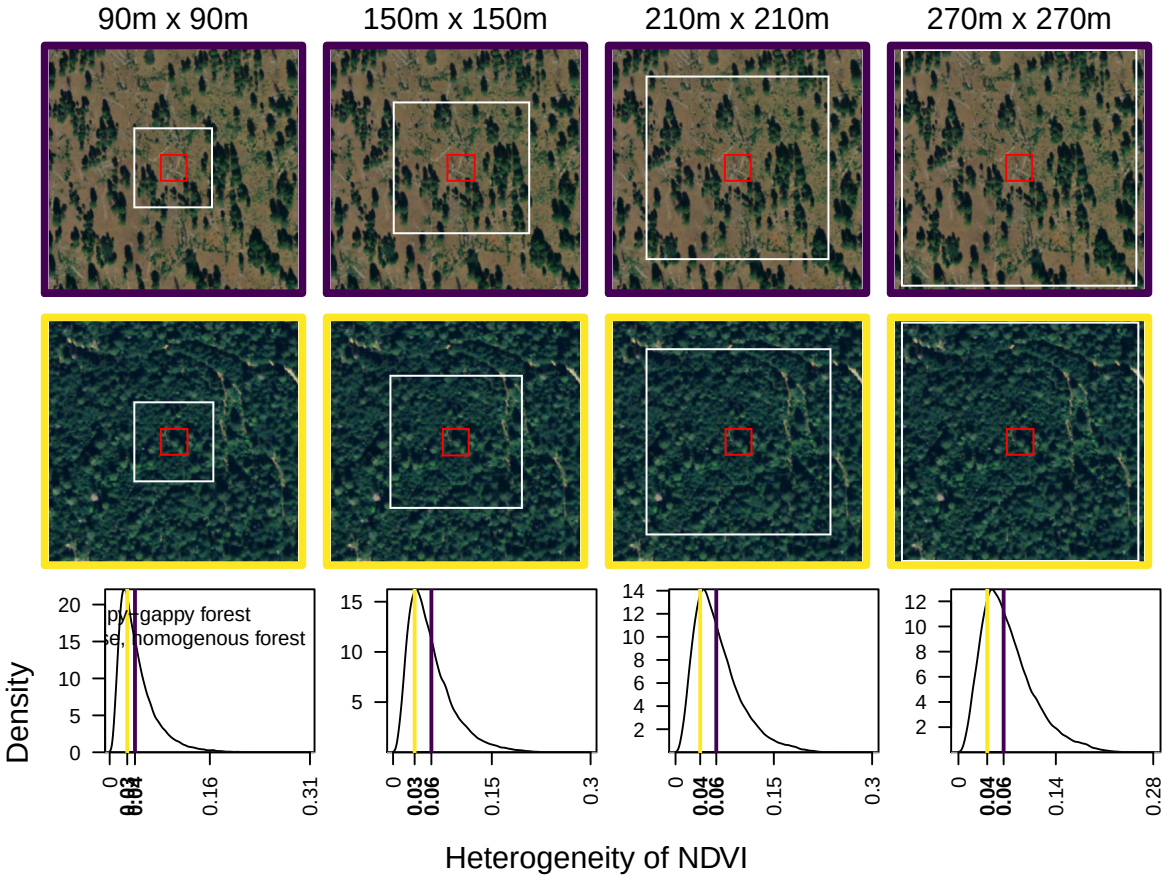

Figure 8: Highly heterogeneous forest in the Beaver Creek Pinery and homogenous forest nearby. Aerial photographs from USDA Farm Service Agency

Discussion

Main points

1. We can programmatically measure severity with high accuracy and minimal user input– just a geometry and a fire alarm date.

2. We echo the conclusion of Zhu *et al.* (2006) that the validation of differences between pre- and postfire NDVI to field measured severity data, which uses near infrared reflectance, is comparable to validation using more commonly used severity metrics (e.g., RdNBR and dNBR) that rely on short wave infrared reflectance. One immediately operational implication of this is that the increasing availability of low-cost small unhumanned aerial systems (sUAS a.k.a. drones) and near infrared detecting imagers (e.g., those used for agriculture monitoring) may be used to measure wildfire severity at very high spatial resolutions.

3. We encourage people to make their on-the-ground severity data available with site location (including datum) and the alarm data for the fire the field data is measuring. Cloud-based GIS, central image hosting, and integration with powerful classification tools are ready right now to train on these data and advance our understanding of wildfire effects on the landscape.

4.

Our method should work best in denser vegetation such as forests, as the signal of a wildfire in other systems can be invisible in a matter of weeks (Goodwin & Collett 2014). This method would also require calibration with field data in other systems, as some severity metrics (such as RBR and RdNBR) have found limited success in other regions (Fernández-García *et al.* 2018).

The heterogeneity measure (standard deviation of NDVI in a 2ha moving window) can be fine-tuned and put into context by cross walking it with imagery at a finer spatial resolution (but with a cost in temporal resolution and time series depth; e.g. NAIP imagery at 1m resolution but with only 3 total images starting in 2008) (Dickinson *et al.* 2016). Additional metrics of heterogeneity such as vegetation patch size distributions or non-vegetated gap size distributions, may also be more tractable using the finer spatial resolution of NAIP imagery, though the specific fires used in these analyses will be limited to those taking place after 2008.

If heterogeneous forests are more resilient to fire, then we expect heterogeneity to be relatively maintained after fire.

The spatial autocorrelation inherent in analyses of spatial processes is an important consideration for model

inference, because it challenges the assumptions of standard statistical techniques.

1.

Abatzoglou, J.T. (2013). Development of gridded surface meteorological data for ecological applications and modelling. *International Journal of Climatology*, 33, 121–131.

2.

Ackerly, D.D., Loarie, S.R., Cornwell, W.K., Weiss, S.B., Hamilton, H. & Branciforte, R. *et al.* (2010). The geography of climate change: Implications for conservation biogeography. *Diversity and Distributions*, 16, 476–487.

3.

Agashe, D. (2009). The stabilizing effect of intraspecific genetic variation on population dynamics in novel and ancestral habitats. *The American Naturalist*, 174, 255–67.

4.

Asner, G.P., Brodrick, P.G., Anderson, C.B., Vaughn, N., Knapp, D.E. & Martin, R.E. (2015). Progressive forest canopy water loss during the 2012–2015 California drought. *Proceedings of the National Academy of Sciences*, 2015, 201523397.

5.

Asner, G.P., Martin, R.E., Knapp, D.E., Tupayachi, R., Anderson, C.B. & Sinca, F. *et al.* (2017). Airborne laser-guided imaging spectroscopy to map forest trait diversity and guide conservation. *Science*, 355, 385–389.

6.

Baskett, M.L., Gaines, S.D. & Nisbet, R.M. (2009). Symbiont diversity may help coral reefs survive moderate climate change. *Ecological Applications*, 19, 3–17.

7.

Bastarrika, A., Chuvieco, E. & Martín, M.P. (2011). Mapping burned areas from landsat TM/ETM+ data with a two-phase algorithm: Balancing omission and commission errors. *Remote Sensing of Environment*, 115, 1003–1012.

8.

Bates, D., Maechler, M., Bolker, B. & Walker, S. (2015). *Fitting linear mixed-effects models using lme4.*

9.

Boschetti, L., Roy, D.P., Justice, C.O. & Humber, M.L. (2015). MODIS-Landsat fusion for large area 30m burned area mapping. *Remote Sensing of Environment*, 161, 27–42.

10.

Cadotte, M., Albert, C.H. & Walker, S.C. (2013). The ecology of differences: Assessing community assembly with trait and evolutionary distances. *Ecology Letters*, 16, 1234–1244.

11.

Cansler, C.A. & McKenzie, D. (2012). How robust are burn severity indices when applied in a new region? Evaluation of alternate field-based and remote-sensing methods. *Remote Sensing*, 4, 456–483.

12.

Chesson, P. (2000). Mechanisms of maintenance of species diversity. *Annual Review of Ecology and Systematics*, 31, 343–366.

13.

Clyatt, K.A., Crotteau, J.S., Schaedel, M.S., Wiggins, H.L., Kelley, H. & Churchill, D.J. *et al.* (2016). Historical spatial patterns and contemporary tree mortality in dry mixed-conifer forests. *Forest Ecology and Management*, 361, 23–37.

14.

Collins, B.M., Lydersen, J.M., Everett, R.G., Fry, D.L. & Stephens, S.L. (2015). Novel characterization of landscape-level variability in historical vegetation structure. *Ecological Applications*, 25, 1167–1174.

15.

Collins, B.M. & Stephens, S.L. (2010). Stand-replacing patches within a 'mixed severity' fire regime: Quantitative characterization using recent fires in a long-established natural fire area. *Landscape Ecology*, 25, 927–939.

16.

Conners, R.W., Trivedi, M.M. & Harlow, C.A. (1984). Segmentation of a high-resolution urban scene using texture operators. *Computer Vision, Graphics, and Image Processing*, 25, 273–310.

17.

Crowther, T.W., Glick, H.B., Covey, K.R., Bettigole, C., Maynard, D.S. & Thomas, S.M. *et al.* (2015). Mapping tree density at a global scale. *Nature*, 525, 201–205.

18.

Culbert, P.D., Radeloff, V.C., St-Louis, V., Flather, C.H., Rittenhouse, C.D. & Albright, T.P. *et al.* (2012). Modeling broad-scale patterns of avian species richness across the Midwestern United States with measures of satellite image texture. *Remote Sensing of Environment*, 118, 140–150.

19.

De Frenne, P., Rodríguez-Sánchez, F., Coomes, D.A., Baeten, L., Verstraeten, G. & Vellend, M. *et al.* (2013). Microclimate moderates plant responses to macroclimate warming. *Proceedings of the National Academy of Sciences of the United States of America*, 110, 18561–5.

20.

De Santis, A., Asner, G.P., Vaughan, P.J. & Knapp, D.E. (2010). Mapping burn severity and burning efficiency in California using simulation models and Landsat imagery. *Remote Sensing of Environment*, 114, 1535–1545.

21.

Dickinson, Y., Pelz, K., Giles, E. & Howie, J. (2016). Have we been successful? Monitoring horizontal forest complexity for forest restoration projects. *Restoration Ecology*, 24, 8–17.

22.

Dillon, G.K., Holden, Z.A., Morgan, P., Crimmins, M.A., Heyerdahl, E.K. & Luce, C.H. (2011). Both topography and climate affected forest and woodland burn severity in two regions of the western US, 1984 to 2006. *Ecosphere*, 2, art130.

23.

Edwards, A.C., Russell-Smith, J. & Maier, S.W. (2018). A comparison and validation of satellite-derived fire severity mapping techniques in fire prone north Australian savannas: Extreme fires and tree stem mortality. *Remote Sensing of Environment*, 206, 287–299.

24.

Eidenshink, J., Schwind, B., Brewer, K., Zhu, Z.-l., Quayle, B. & Howard, S. (2007). A project for monitoring trends in burn severity. *Fire Ecology*, 3, 3–21.

25.

Farr, T., Rosen, P., Caro, E., Crippen, R., Duren, R. & Hensley, S. *et al.* (2007). The shuttle radar topography mission. *Reviews of Geophysics*, 45, 1–33.

26.

Fernández-García, V., Santamarta, M., Fernández-Manso, A., Quintano, C., Marcos, E. & Calvo, L. (2018). Burn severity metrics in fire-prone pine ecosystems along a climatic gradient using Landsat imagery. *Remote Sensing of Environment*, 206, 205–217.

27.

Folke, C., Carpenter, S., Walker, B., Scheffer, M., Elmqvist, T. & Gunderson, L. *et al.* (2004). Regime shifts, resilience, and biodiversity in ecosystem management. *Annual Review of Ecology, Evolution, and Systematics*, 35, 557–581.

28.

Ford, K.R., Ettinger, A.K., Lundquist, J.D., Raleigh, M.S. & Hille Ris Lambers, J. (2013). Spatial heterogeneity in ecologically important climate variables at coarse and fine scales in a high-snow mountain landscape. *PLoS ONE*, 8, e65008.

29.

Fry, D.L., Stephens, S.L., Collins, B.M., North, M.P., Franco-Vizcaíno, E. & Gill, S.J. (2014). Contrasting spatial patterns in active-fire and fire-suppressed Mediterranean climate old-growth mixed conifer forests. *PLoS ONE*, 9, e88985.

30.

Gao, B.C. (1996). NDWI - A normalized difference water index for remote sensing of vegetation liquid water from space. *Remote Sensing of Environment*, 58, 257–266.

31.

Gazol, A. & Camarero, J.J. (2016). Functional diversity enhances silver fir growth resilience to an extreme drought. *Journal of Ecology*.

32.

Goodwin, N.R. & Collett, L.J. (2014). Development of an automated method for mapping fire history captured in Landsat TM and ETM+ time series across Queensland, Australia. *Remote Sensing of Environment*, 148, 206–221.

33.

Gorelick, N., Hancher, M., Dixon, M., Ilyushchenko, S., Thau, D. & Moore, R. (2017). Remote Sensing of Environment Google Earth Engine : Planetary-scale geospatial analysis for everyone. *Remote Sensing of Environment*, 202, 18–27.

34.

Graham, R.T., McCaffrey, S. & Jain, T.B. (2004). *Science basis for changing forest structure to modify wildfire behavior and severity* (No. April). US Department of Agriculture, Forest Service, Rokcy Mountain Research Station, Fort Collins, CO.

35.

438 Gunderson, L.H. (2000). Ecological resilience– in theory and application. *Annual Review of Ecology and*
439 *Systematics*, 31, 425–439.

440 36.

441 Hansen, M.C., Potapov, P.V., Moore, R., Hancher, M., Turubanova, S.A. & Tyukavina, A. (2013). High-
442 resolution global maps of 21st-century forest cover change. *Science*, 342, 850–853.

443 37.

444 Haralick, R.M., Shanmugam, K. & Dinstein, I. (1973). Textural Features for Image Classification. *IEEE*
445 *Transactions on Systems, Man, and Cybernetics*, SMC-3, 610–621.

446 38.

447 Hawbaker, T.J., Vanderhoof, M.K., Beal, Y.J., Takacs, J.D., Schmidt, G.L. & Falgout, J.T. *et al.* (2017).
448 Mapping burned areas using dense time-series of Landsat data. *Remote Sensing of Environment*, 198, 504–522.

449 39.

450 Holden, Z.A., Morgan, P. & Evans, J.S. (2009). A predictive model of burn severity based on 20-year satellite-
451 inferred burn severity data in a large southwestern US wilderness area. *Forest Ecology and Management*, 258,
452 2399–2406.

453 40.

454 Holling, C.S. (1973). Resilience and Stability of Ecological Systems. *Annual Review of Ecology and Systematics*,
455 4, 1–23.

456 41.

457 Huang, Q., Swatantran, A., Dubayah, R. & Goetz, S.J. (2014). The influence of vegetation height heterogeneity
458 on forest and woodland bird species richness across the United States. *PLoS ONE*, 9.

459 42.

460 Keeley, J.E., Pausas, J.G., Rundel, P.W., Bond, W.J. & Bradstock, R.A. (2011). Fire as an evolutionary
461 pressure shaping plant traits. *Trends in Plant Science*, 16, 406–11.

462 43.

463 Key, C.H. & Benson, N.C. (2006). Landscape assessment: Sampling and analysis methods. *USDA Forest*
464 *Service General Technical Report RMRS-GTR-164-CD*, 1–55.

465 44.

466 Kolden, C.A., Smith, A.M.S. & Abatzoglou, J.T. (2015). Limitations and utilisation of Monitoring Trends in
467 Burn Severity products for assessing wildfire severity in the USA. *International Journal of Wildland Fire*, 24,

1023–1028.

45.

Kotliar, N.B. & Wiens, J. a. (1990). Multiple Scales of Patchiness and Patch Structure: A Hierarchical Framework for the Study of Heterogeneity. *Oikos*, 59, 253–260.

46.

Larson, A.J. & Churchill, D. (2012). Tree spatial patterns in fire-frequent forests of western North America, including mechanisms of pattern formation and implications for designing fuel reduction and restoration treatments. *Forest Ecology and Management*, 267, 74–92.

47.

Lenoir, J., Graae, B.J., Aarrestad, P.A., Alsos, I.G., Armbruster, W.S. & Austrheim, G. *et al.* (2013). Local temperatures inferred from plant communities suggest strong spatial buffering of climate warming across Northern Europe. *Global Change Biology*, 19, 1470–1481.

48.

Lydersen, J.M., North, M.P., Knapp, E.E. & Collins, B.M. (2013). Quantifying spatial patterns of tree groups and gaps in mixed-conifer forests: Reference conditions and long-term changes following fire suppression and logging. *Forest Ecology and Management*, 304, 370–382.

49.

Mandle, L., Bufford, J.L., Schmidt, I.B. & Daehler, C.C. (2011). Woody exotic plant invasions and fire: Reciprocal impacts and consequences for native ecosystems. *Biological Invasions*, 13, 1815–1827.

50.

Masek, J.G., Vermote, E.F., Saleous, N.E., Wolfe, R., Hall, F.G. & Huemmrich, K.F. *et al.* (2006). A Landsat Surface Reflectance Dataset. *IEEE Geoscience and Remote Sensing Letters*, 3, 68–72.

51.

McCune, B. (2007). Improved estimates of incident radiation and heat load using non-parametric regression against topographic variables. *Journal of Vegetation Science*, 18, 751–754.

52.

McCune, B. & Keon, D. (2002). Equations for potential annual direct incident radiation and heat load. *Journal of Vegetation Science*, 13, 603–606.

53.

Millar, C.I. & Stephenson, N.L. (2015). Temperate forest health in an era of emerging megadisturbance.

Science, 349, 823–826.

54.

Millar, C.I., Stephenson, N.L. & Stephens, S.L. (2007). Climate change and forests of the future: Managing in the face of uncertainty. *Ecological Applications*, 17, 2145–2151.

55.

Miller, J.D., Knapp, E.E., Key, C.H., Skinner, C.N., Isbell, C.J. & Creasy, R.M. *et al.* (2009). Calibration and validation of the relative differenced Normalized Burn Ratio (RdNBR) to three measures of fire severity in the Sierra Nevada and Klamath Mountains, California, USA. *Remote Sensing of Environment*, 113, 645–656.

56.

Miller, J.D. & Thode, A.E. (2007). Quantifying burn severity in a heterogeneous landscape with a relative version of the delta Normalized Burn Ratio (dNBR). *Remote Sensing of Environment*, 109, 66–80.

57.

Moritz, M.A., Morais, M.E., Summerell, L.A., Carlson, J.M. & Doyle, J. (2005). Wildfires, complexity, and highly optimized tolerance. *Proceedings of the National Academy of Sciences*, 102, 17912–7.

58.

Näsi, R., Honkavaara, E., Lyytikäinen-Saarenmaa, P., Blomqvist, M., Litkey, P. & Hakala, T. *et al.* (2015). Using UAV-based photogrammetry and hyperspectral imaging for mapping bark beetle damage at tree-level. *Remote Sensing*, 7, 15467–15493.

59.

North, M.P., Stephens, S.L., Collins, B.M., Agee, J.K., Aplet, G. & Franklin, J.F. *et al.* (2015). Reform forest fire managment. *Science*, 349, 1280–1281.

60.

North, M., Stine, P., Hara, K.O., Zielinski, W. & Stephens, S. (2009). An Ecosystem Management Strategy for Sierran Mixed- Conifer Forests. *General Technical Report PSW-GTR-220*, 1–49.

61.

Park Williams, A., Allen, C.D., Macalady, A.K., Griffin, D., Woodhouse, C.A. & Meko, D.M. *et al.* (2012). Temperature as a potent driver of regional forest drought stress and tree mortality. *Nature Climate Change*, 3, 292–297.

62.

Parks, S.A., Dillon, G.K. & Miller, C. (2014). A new metric for quantifying burn severity: The relativized

528 burn ratio. *Remote Sensing*, 6, 1827–1844.

529 63.

530 Prichard, S.J. & Kennedy, M.C. (2014). Fuel treatments and landform modify landscape patterns of burn
531 severity in an extreme fire event. *Ecological Applications*, 24, 571–590.

532 64.

533 Questad, E.J. & Foster, B.L. (2008). Coexistence through spatio-temporal heterogeneity and species sorting
534 in grassland plant communities. *Ecology Letters*, 11, 717–726.

535 65.

536 R Core Team. (2017). *R: A language and environment for statistical computing. http://www.r-project.org/.*
537 R Foundation for Statistical Computing, Vienna, Austria.

538 66.

539 Raffa, K.F., Aukema, B., Bentz, B.J., Carroll, A., Erbilgin, N. & Herms, D.A. *et al.* (2009). A literal use of
540 'forest health' safeguards against misuse and misapplication. *Journal of Forestry*, 276–277.

541 67.

542 Raffa, K.F., Aukema, B.H., Bentz, B.J., Carroll, A.L., Hicke, J.A. & Turner, M.G. *et al.* (2008). Cross-scale
543 drivers of natural disturbances prone to anthropogenic amplification: The dynamics of bark beetle eruptions.
544 *BioScience*, 58, 501.

545 68.

546 Reilly, M.J., Dunn, C.J., Meigs, G.W., Spies, T.A., Kennedy, R.E. & Bailey, J.D. *et al.* (2017). Contemporary
547 patterns of fire extent and severity in forests of the Pacific Northwest, USA (1985-2010). *Ecosphere*, 8.

548 69.

549 Reusch, T.B.H., Ehlers, A., Hämmerli, A. & Worm, B. (2005). Ecosystem recovery after climatic extremes
550 enhanced by genotypic diversity. *Proceedings of the National Academy of Sciences*, 102, 2826–2831.

551 70.

552 Rouse, J.W., Hass, R.H., Schell, J. & Deering, D. (1973). Monitoring vegetation systems in the great plains
553 with ERTS. *Third Earth Resources Technology Satellite (ERTS) symposium*, 1, 309–317.

554 71.

555 Scheffer, M., Carpenter, S., Foley, J.A., Folke, C. & Walker, B. (2001). Catastrophic shifts in ecosystems.
556 *Nature*, 413, 591–596.

557 72.

Scholl, A.E. & Taylor, A.H. (2010). Fire regimes, forest change, and self-organization in an old-growth mixed-conifer forest, Yosemite National Park, USA. *Ecological Applications*, 20, 362–380.

73.

Sikkink, P.G., Dillon, G.K., Keane, R.E., Morgan, P., Karau, E.C. & Holden, Z.A. *et al.* (2013). *Composite Burn Index (CBI) data and field photos collected for the FIRESEV project, western United States.* Forest Service Research Data Archive, Fort Collins, CO.

74.

Steel, Z.L., Safford, H.D. & Viers, J.H. (2015). The fire frequency-severity relationship and the legacy of fire suppression in California forests. *Ecosphere*, 6, 1–23.

75.

Stein, A., Gerstner, K. & Kreft, H. (2014). Environmental heterogeneity as a universal driver of species richness across taxa, biomes and spatial scales. *Ecology Letters*, 17, 866–880.

76.

Stephens, S.L. & Collins, B.M. (2004). Fire regimes of mixed conifer forests in the North-Central Sierra Nevada at multiple scales. *Northwest Science*, 78, 12–23.

77.

Stephens, S.L., Fry, D.L. & Franco-Vizcaíno, E. (2008). Wildfire and spatial patterns in forests in northwestern Mexico: The United States wishes it had similar fire problems. *Ecology and Society.*

78.

Stephens, S.L., Lydersen, J.M., Collins, B.M., Fry, D.L. & Meyer, M.D. (2015). Historical and current landscape-scale ponderosa pine and mixed conifer forest structure in the Southern Sierra Nevada. *Ecosphere*, 6, 1–63.

79.

Stephens, S.L., Moghaddas, J.J., Edminster, C., Fiedler, C.E., Haase, S. & Harrington, M. *et al.* (2013). Fire Treatment Effects on Vegetation Structure, Fuels, and Potential Fire Severity in Western U. S. Forests. *Ecological Applications*, 19, 305–320.

80.

Sugihara, N.G. & Barbour, M.G. (2006). Fire and California vegetation. In: *Fire in california's ecosystems* (eds. Sugihara, N.G., Van Wagtendonk, J.W., Shaffer, K.E., Fites-Kaufman, J. & Thode, A.E.). University of California Press, Berkeley; Los Angeles, CA, USA, pp. 1–9.

588 81.

589 Tilman, D. (1994). Competition and biodiversity in spatially structured habitats. *Ecology*, 75, 2–16.

590 82.

591 Trumbore, S., Brando, P. & Hartmann, H. (2015). Forest health and global change. *Science*, 349.

592 83.

593 Tuanmu, M.-N. & Jetz, W. (2015). A global, remote sensing-based characterization of terrestrial habitat
594 heterogeneity for biodiversity and ecosystem modelling. *Global Ecology and Biogeography*, n/a–n/a.

595 84.

596 Turner, M.G., Donato, D.C. & Romme, W.H. (2013). Consequences of spatial heterogeneity for ecosystem
597 services in changing forest landscapes: Priorities for future research. *Landscape Ecology*, 28, 1081–1097.

598 85.

599 USGS. (2017a). Product Guide: Landat 8 Surface Reflectance Code (LaSRC) Product. *USGS Professional*
600 *Paper*, 4.2.

601 86.

602 USGS. (2017b). Product Guide: Landsat 4-7 Surface Reflectance (LEDAPS) Product. *USGS Professional*
603 *Paper*, 8, 38.

604 87.

605 Veraverbeke, S. & Hook, S.J. (2013). Evaluating spectral indices and spectral mixture analysis for assessing
606 fire severity, combustion completeness and carbon emissions. *International Journal of Wildland Fire*, 22,
607 707–720.

608 88.

609 Vermote, E., Justice, C., Claverie, M. & Franch, B. (2016). Preliminary analysis of the performance of the
610 Landsat 8/OLI land surface reflectance product. *Remote Sensing of Environment*, 185, 46–56.

611 89.

612 Virah-Sawmy, M., Willis, K.J. & Gillson, L. (2009). Threshold response of Madagascar's littoral forest to
613 sea-level rise. *Global Ecology and Biogeography*, 18, 98–110.

614 90.

615 Walker, B., Holling, C.S., Carpenter, S.R. & Kinzig, A. (2004). Resilience, adaptability, and transformability
616 in social-ecological systems. *Ecology and Society*, 9, 5.

617 91.

618 Westerling, A.L., Hidalgo, H.G., Cayan, D.R. & Swetnam, T.W. (2006). Warming and earlier spring increase
619 western U.S. forest wildfire activity. *Science*, 313, 940–943.

620 92.

621 Wood, E.M., Pidgeon, A.M., Radeloff, V.C. & Keuler, N.S. (2012). Image texture as a remotely sensed
622 measure of vegetation structure. *Remote Sensing of Environment*, 121, 516–526.

623 93.

624 Young, D.J.N., Stevens, J.T., Earles, J.M., Moore, J., Ellis, A. & Jirka, A.L. *et al.* (2017). Long-term climate
625 and competition explain forest mortality patterns under extreme drought. *Ecology Letters*, 20, 78–86.

626 94.

627 Zhu, Z., Key, C., Ohlen, D. & Benson, N. (2006). Evaluate Sensitivities of Burn-Severity Mapping Algorithms
628 for Different Ecosystems and Fire Histories in the United States. *Final Report to the Joint Fire Science*
629 *Program, Project JFSP 01-1-4-12*, 1–35.